HHS Public Access

Author manuscript

ACS Synth Biol. Author manuscript; available in PMC 2023 July 18.

Published in final edited form as:

ACS Synth Biol. 2019 June 21; 8(6): 1314–1324. doi:10.1021/acssynbio.8b00528.

Engineering adenylate cyclase activated by near-infrared window light for mammalian optogenetic applications

Anastasia Fomicheva[1], **Chen Zhou**[2], **Qian-Quan Sun**[2], **Mark Gomelsky**[1,*]

[1]Department of Molecular Biology, University of Wyoming, Laramie, Wyoming 82071, USA

[2]Department of Zoology and Physiology, University of Wyoming, Laramie, Wyoming 82071, USA

Abstract

Light in the near-infrared optical window (NIRW) penetrates deep through mammalian tissues, including the skull and brain tissue. Here we engineered an adenylate cyclase (AC) activated by NIRW light (NIRW-AC) and suitable for mammalian applications. To accomplish this goal, we constructed fusions of several bacteriophytochrome photosensory and bacterial AC modules using guidelines for designing chimeric homodimeric bacteriophytochromes. One engineered NIRW-AC, designated IlaM5, has significantly higher activity at 37 °C, is better expressed in mammalian cells, and can mediate cAMP-dependent photoactivation of gene expression in mammalian cells, in favorable contrast to the NIRW-ACs engineered earlier. The *ilaM5* gene expressed from an AAV vector was delivered into the ventral basal thalamus region of the mouse brain resulting in the light-controlled suppression of the cAMP-dependent wave pattern of the sleeping brain known as spindle oscillations. Reversible spindle oscillation suppression was observed in sleeping mice exposed to light from an external light source. This study confirms robustness of principles of homodimeric bacteriophytochrome engineering, describes a NIRW-AC suitable for mammalian optogenetic applications, and demonstrates feasibility of controlling brain activity via NIRW-ACs using transcranial irradiation.

Keywords

optogenetics; cAMP; adenylate cyclase; neuron; sleep; spindle oscillation

The near-infrared optical window (NIRW) encompasses the spectral region of ~670–900 nm[1], at the border of the far-red light and the near-infrared light. NIRW light penetrates through mammalian tissues much deeper than the visible light of shorter wavelengths[2,3], therefore it can be used to control biological activities at the depth of several cm[4]. It is also

[*]**Corresponding Author:** Tel. +1 (307) 766-3522; gomelsky@uwyo.edu.

Author Contributions

A.F. designed and carried out the experiments, made figures, performed data analysis pertaining to protein engineering, bacterial and cell culture measurements, and wrote the initial draft of the manuscript. C.Z. carried out the experiments, made figures, performed data analysis pertaining to mouse experiments and contributed to writing the initial draft of the manuscript. M.G. and Q.S. conceived the project, designed the experiments, analyzed the data, and wrote the manuscript.

M.G. is one of the inventors on US Patent 8835399 and European Patent EP 2737062 (owned by University of Wyoming) that describe engineering of the homodimeric near-infrared light-activated proteins. Other authors declare no competing financial interests.

Supporting Information. Table S1 listing bacterial strains and plasmids and Figures S1–S6 supporting main figures, results and discussion (PDF).

remarkably safe, as demonstrated by the multi-decade medical practice of transcranial laser photobiostimulation and phototherapy[5]. To harness the power of NIRW light, our group and other researchers have engineered optogenetic tools involving bacteriophytochrome (Bph) photoreceptors[6] that sense light in the 670–760 nm spectral region. The Bph chromophore, biliverdin IXα (BV), is ubiquitously present in mammalian tissues as the first product of heme turnover, therefore it needs not be delivered to mammals[7]. A NIRW photon induces BV isomerization leading to the conversion of the inactive dark state of the Bph to the lit state. The dark state is usually red light-absorbing, P_r, while the lit state is absorbing far-red light, P_{fr}; however, the so-called bathy-Bphs have the opposite arrangement[6]. The conversion from the lit to the more stable dark state (dark reversion) occurs gradually, in a timescale of seconds to hours, dependent on the Bph species. This conversion can be greatly accelerated by irradiating the lit state with light of the appropriate wavelength[6].

Naturally occurring Bphs exist as homodimers that usually possess histidine kinase or diguanylate cyclase activities[6]. In the inhibited, dark state, two enzymatic domain monomers are misaligned. Light triggers conformational changes in the photosensory (PSM) modules that bring the enzymatic domains together to form a catalytic center at the monomer interface[6,7]. We previously described an approach for engineering Bphs with non-native, heterologous activities, and designed adenylate cyclases (ACs) activated by NIRW light, NIRW-ACs[8]. Like histidine kinases and diguanylate cyclases, bacterial type III ACs function as homodimers, where conversion of ATP to cAMP takes place at the interface of two monomeric AC-domains[9]. The first generation NIRW-ACs, IlaC-series, were constructed as fusions of the PSM of the *Rhodobacter sphaeroides* Bph, BphG1[10], and the catalytic domain of the class III AC from *Nostoc* sp., CyaB1[11] (Figure 1a, 1b). The IlaC enzymes enabled photoactivation of (i) the cAMP-dependent gene expression in *Escherichia coli* at 30 °C and (ii) neuronal activity in *C. elegans* at room temperature[12]. Unfortunately, they proved inadequate for regulating gene expression in human cells, as documented in this study, or neuronal activity in mice[13]. The impetus for this work was to identify the deficiencies of the first-generation NIRW-ACs and to engineer enzymes suitable for optogenetic applications in mammals.

The range of potential applications of NIRW-ACs is vast because in mammals, cAMP-dependent signaling pathways regulate a variety of important processes such as learning and memory formation, insulin synthesis in the pancreas, heartbeat frequency, lipolysis in adipose tissue, and water secretion in the gastrointestinal tract[14]. Abnormal cAMP signaling has been associated with numerous pathologies. Therefore, in the past decades, significant strides have been made toward developing drugs that modulate cAMP signaling, i.e. inhibitors of specific cAMP phosphodiesterases and activators of ACs. The lead compounds have been tested for the treatment of Alzheimer and Parkinson disease, schizophrenia, substance dependence disorders, as well as cardiovascular, inflammatory, and metabolic disorders[15–18]. However, thus far very few clinically approved medications have emerged from these studies. The major challenge in pharmacological approaches is the lack of cell type and tissue specificity that leads to undesired side effects in non-target tissues. Yet another major limitation is the inability of drugs to capture the temporary nature of cAMP signaling[16]. The optogenetic mode of regulating cAMP signaling may overcome these

limitations if an AC encoding gene is expressed in specific cells where the NIRW-AC can be turned on and off in a spatially- and temporally controlled manner.

RESULTS AND DISCUSSION

Engineering of the next generation NIRW-ACs.

To understand why the IlaC-series NIRW-ACs failed in applications in mammals, we analyzed expression and activity in human cells of the best-performing first generation NIRW-AC, IlaC22 k27 Y259F[12] (abbreviated here as IlaC*). Because IlaC* is poorly expressed in *E. coli* (Figure 2a), we suspected that its expression in human cells may also be low. This prediction proved to be correct, i.e. the IlaC*::His_6 protein was undetectable in the HEK293 cells when assayed by immunoblotting using His_6-specific antibodies (Figure 2b). Therefore, our first goal was to improve NIRW-AC expression in mammalian cells. To increase expression, we replaced the PSM module of IlaC*, that originated from BphG1, with the PSM from the *Deinococcus radiodurans* BphP (Figures 1a, 1b), known to be highly expressed in *E. coli*[19,20]. Yet another feature of BphP that attracted our interest was its slow dark (P_{fr} to P_r) reversion[21]. A NIRW-AC with a long-lived lit state was expected to retain its enzymatic activity *in vivo* for extended periods of time thus allowing to maintain elevated cAMP levels in cells via infrequent light pulses, as opposed to constant irradiation. This feature would be particularly valuable for applications in deep tissues poorly accessible by light.

We fused the PSM of *D. radiodurans* BphP truncated at the α-helix (connecting the PSM and histidine kinase modules) to the first structural element, β-strand, of the *Nostoc* sp. CyaB1 AC (Figures 1a, 1b, Supplementary Figure 1). In the fusion proteins, designated IlaD3 and IlaD1, we used the same lengths of the α-helical linkers as in IlaC* and IlaC25, another first-generation NIRW-AC[12] (Figure 1c). An additional fusion, designated IlaD2, contained the linker that was shorter by 1 aa, compared to IlaD1 (Figure 1c). The AC activities of the engineered chimeric proteins were evaluated by monitoring cAMP-dependent expression of the chromosomal *lacZ* gene in the *E. coli cya* mutant, which lacks its native AC gene[12] (Figure 3a). IlaD1 showed constitutive, light-independent AC activity, IlaD3 showed modest photoactivation (photodynamic range), and IlaD2 was inactive. In our earlier work, we showed that an extension of the linker by approximately one (3 or 4 aa), two (7 or 8 aa) or more α-helical turns often preserves light-dependent properties of the fusions[12]. The likely reason is that such extensions preserve the ‘phase’ at which the AC domains face each other upon formation of a catalytically active site at the homodimer interface[8,12] (Figure 1b). Following this line of reasoning, we extended the α-helical linker in IlaD3 by 3 and 4 aa (approximately 1 α-helical turn) using residues from the α-helical linker present in the ACs of the IlaC-series (Figure 1c). The IlaD3 protein containing a 3-aa extension, designated IlaD9, had higher photodynamic range than IlaD3 in *E. coli cya* (Supplementary Figure 2a), therefore it was characterized further. It is noteworthy that IlaD9 contains the same linker sequence and length as the photoactivated IlaC17 from the IlaC-series[12].

In accord with our expectations, expression of IlaD9 in *E. coli* was drastically increased, compared to IlaC* (Figure 2a) and stability of its lit state was also increased. Therefore, it

was possible to maintain high cAMP-dependent *lacZ* expression in *E. coli* colonies that were exposed to infrequent light pulses interspersed with long periods of darkness (0.5 min light/ 30 min dark). To reach similar levels of *lacZ* expression, *E. coli* expressing IlaC* had to be irradiated much more frequently, i.e. 0.5 min light/ 2 min dark (Figure 3b). Unfortunately, superior performance of IlaD9, compared to IlaC*, was evident only when *E. coli* were grown at 28 but not at 37 °C (Figure 3b). This result suggests that AC activity of the catalytic domain of cyanobacterial CyaB1 may be limiting its activity at 37 °C.

In the next round of engineering, we replaced the AC domain of CyaB1 in IlaD9 with the AC domain from Rv1264 (Supplementary Figure 1b), an AC from *Mycobacterium tuberculosis*[22] (Figure 1a, c). Given that *M. tuberculosis* is a human pathogen, we expected Rv1264 to maintain high AC activity at 37 °C. The engineered fusion protein IlaM1 contained the same α-helical linker as the linker in IlaD9 (Figure 1c, Supplementary Figure 1b), yet it possessed constitutive, light-independent AC activity (Supplementary Figure 2b). We, therefore, constructed another protein, IlaM4, that had the same linker length as IlaM1 but a different fusion site, 4 aa into the β-strand from the AC domain of CyaB1 (Figure 1c). We expected this construct to preserve the transition from the α-helical linker to the β-strand of the AC that worked in the light-activated IlaD9 protein. The NIRW-AC activity of IlaM4 indeed proved to be light-activated (Figure 3b). Next, we shortened and extended the α-helical linker in IlaM4 by 1 aa and found that a 1-aa extension produced another light-activated enzyme, IlaM5, whose AC activity in the lit state was higher, compared to the activity of IlaM4 (Figure 3b and Supplementary Figure 2c). Successful engineering of NIRW-ACs from different PSMs and AC modules supports the notion that design principles for constructing homodimeric Bphs are robust[8,12].

Similar to IlaD9, IlaM5 was highly expressed in *E. coli*, suggesting that expression levels are primarily determined by the PSM, not AC, module (Figure 2a). In favorable contrast to IlaD9, IlaM5 had significantly higher AC activity at 37 °C (Figure 3b), which was the goal of our engineering efforts. Further, maintaining cAMP synthesis in *E. coli* required only infrequent irradiation (0.5 min light/ 30 min dark), as was expected from a NIRW-AC with the PSM that has slow dark reversion. Higher expression and activity at 37 °C, compared to the enzymes of the IlaC- and IlaD-series, warranted further characterization of IlaM5 *in vitro* and in mammalian cells.

Characterization of the engineered NIRW-ACs *in vitro*.

To characterize activities of the NIRW-ACs *in vitro*, we expressed the C-terminal His_6-tagged fusions of IlaM5, IlaM4, IlaD9 and IlaC* in *E. coli* and purified these proteins by affinity chromatography. AC activities were measured at room temperature (22 °C) and at 37 °C, in the dark and under activating red (660 nm) light. Irradiation increased the initial AC activity of IlaC* by 6.3 ± 0.5-fold at 22 °C (mean ± SD from 3 independent experiments), in accord with our earlier report[12]. Approximately the same photodynamic range, 5.2 ± 0.5-fold, was observed at 37 °C. However, cAMP accumulation over an extended incubation period (30 min) was lower at 37 °C compared to 22 °C (Figure 4a). AC activity of IlaD9 in the light at 22 °C was higher than that of IlaC*. However, it suffered from the same problem as IlaC*, i.e. cAMP accumulation over an extended incubation period (30 min) was also

lower at 37 °C compared to 22 °C (Figure 4a). This finding explains why IlaD9 did not perform better than IlaC* in *E. coli* at 37 °C (Figure 3b).

The photodynamic ranges of IlaM4 and IlaM5 were, respectively, 4.8 ± 0.8-fold and 6.3 ± 1.5-fold at 22 °C and 3.5 ± 0.4-fold and 5.5 ± 0.5-fold at 37 °C (Figure 4a). Their relative activities were significantly higher, compared to the NIRW-ACs containing the AC domain from CyaB1 (Figure 4a). For example, the amount of cAMP synthesized by IlaM5 *in vitro* at 37 °C after a 5-min irradiation pulse was 14-fold higher than the amount of cAMP produced by IlaC* (Figure 4a). The spectral properties of IlaM5 (P_r, 700 nm; P_{fr}, 747 nm; Figure 4b) were similar to the properties reported for *D. radiodurans* BphP (P_r, 700 and P_{fr}, 754 nm)[21]. The half-life of the lit to dark state reversion for IlaM5 at 22 °C was ~400 min (Figure 4c), indicative of a very stable lit state *in vitro*. The drastically improved performance of IlaM5 at 37 °C in *E. coli* and *in vitro*, compared to other NIRW-ACs, confirmed its potential suitability for mammalian cells.

Testing engineered NIRW-ACs in mammalian cell culture.

We compared expression of the IlaM5 and IlaC* proteins in the human embryonic kidney HEK293 cells. The C-terminal His_6-tagged fusions of IlaM5 (pAAV::ilaM5) and IlaC* (pAAV::ilaC*) were cloned in an adeno-associated viral (AAV) vector downstream of the hSyn promoter (Figure 5b). While this promoter is relatively weak in the HEK293 cells due to inhibition by neuron-restrictive silencing factor (REST/NRSF)[23], it had sufficient activity to drive expression of the *eGFP* gene placed downstream of the NIRW-AC genes and separated by the self-cleaving peptide sequence p2A (Supplementary Figure 3a). In the HEK293 cell extracts, the IlaM5::His_6 protein was readily detectable, while IlaC*::His_6 was not, which is consistent with poorer expression of IlaC* in *E. coli* (Figures 2a, 2b).

Next, we tested whether higher activity *in vitro* and better expression in the HEK293 cells has translated into superior photoactivated cAMP synthesis by IlaM5. Light-induced changes in intracellular cAMP levels were assessed via a secreted luciferase reporter[24] expressed from a synthetic cAMP-dependent promoter (Figure 5a), plasmid pCRE-MetLuc2. The HEK293 cells were cotransfected with pCRE-MetLuc2 and either pAAV::ilaM5 or pAAV::ilaC* (Figure 5b). Twenty-four hours post transfection, the media was changed, and cells were grown in the dark or under pulsed (1 min light/ 5 min dark) red (660 nm) light. After a 3-h period of pulsed irradiation, secreted luciferase levels in the irradiated cells transfected with pAAV::IlaM5 were increased by 19-fold, compared to the cells grown in the dark, where luciferase expression remained at the background level. In the cells expressing IlaC*, luciferase levels were also increased, but only by 3-fold (Figure 5c). This result suggests that IlaM5 is suitable for application in mammalian cells.

Upon prolonged irradiation, luciferase levels in the irradiated culture continued to rise, yet the apparent photodynamic range shrunk due to luciferase accumulation in the growth medium (Figure 5c). Note that native ACs of the HEK293 cells contribute to luciferase accumulation even in the absence of NIRW-ACs (Supplementary Fig. 3b). Another noteworthy point is that our AAV constructs contained the *bphO* gene encoding the BV producing heme oxygenase. Inclusion of *bphO* was likely unnecessary because, according to recent studies, endogenous BV levels in mammalian cells, including neurons, are sufficient

for assembly of holo-Bph proteins[7]. The superior performance of IlaM5 in photoactivating cAMP-dependent gene expression in the HEK293 cells, as compared to IlaC*, encouraged us to assess its performance in a mouse model.

Transcranial neuronal photoactivation via an engineered NIRW-AC in mice.

We tested the effect of IlaM5 on spindle oscillations in mice. Spindle oscillations consist of a distinctive, brief pattern of 8- to 15-Hz electroencephalographic (EEG) waves that are generated by the thalamic neurons and occur predominantly during light stages of non-rapid eye movement sleep (NREMS)[27]. Spindle-generating neuronal circuits reside in the intrathalamic network of nucleus reticularis cells and thalamocortical cells. Since spindle oscillations are dependent on the current of hyperpolarized cyclic nucleotide (HCN)-dependent ion channels, I_h[27], we expected that light-induced IlaM5-mediated cAMP accumulation may inhibit spindle oscillations.

To examine the effect of IlaM5, we injected mice with AAV::ilaM5 or saline and conducted EEG recordings. *Post hoc* histological examination verified that the GFP protein, which was cotranslated with IlaM5, was robustly expressed within the ventral posteromedial (VPM) nucleus as well as the nucleus reticularis (Supplementary Figure 4). Screw-free, wire-based intracranial electrodes were implanted in the barrel cortex to record EEG sleep waves. During the NREMS period, after a stable baseline of spindle waves were observed, NIRW light emitted from an LED panel located 30 cm above the mouse cage floor (Supplementary Figure 5) was turned on, and the effects on the EEG waves were examined (Figure 6a). LED irradiation had no effect on spindles in the sham mice (Figures 6b, 6d). In contrast, 2-to-5 min irradiation of the IlaM5-expressing mice resulted in significant reduction in the EEG power-spectrum (6 mice; $P < 0.05$) in between the alpha (47%) and sigma (56%) bands (Figures 6f, 6g), and spindle waves were essentially eliminated (Figures 6b–e). Soon after termination of irradiation, spindle oscillations were fully restored to the pre-irradiation values (Figures 6c, 6e). The subsequent irradiation cycles resulted in essentially the same outcomes.

The relatively fast restoration of spindle waves in the dark was unexpected. Because the lit, P_{fr}, state of IlaM5 is stable *in vitro* (Figure 4c), we expected much slower decrease in cAMP levels and therefore slower restoration of spindle oscillations. We speculate that stability of the lit form of IlaM5 may not be as high *in vivo* as it is *in vitro*, or cAMP turnover in neurons may be very efficient due to neuronal cAMP phosphodiesterases. While unexplained, fast restoration of spindle waves in this system is advantageous as it allows more precise temporal control of neuronal activity.

Unfortunately, the effect of IlaM5 on spindle oscillations proved not to be as specific as desired. First, EEG waves in the IlaM5-expressing mice were partially suppressed even in the absence of irradiation. This observation suggests that expression level of IlaM5 from AAV::ilaM5 in the thalamic neurons needs to be optimized. Second, EEG waves outside of the 8- to 15-Hz spindle wave range were affected by IlaM5 (compare Figures 6b and 6c; 6d and 6e). To decrease nonspecific effects, it could be advantageous to tether IlaM5 to the cytoplasmic membrane thus bringing it closer to the targets of cAMP regulation, the HCN

ion channels. The presented results, however, show feasibility of using IlaM5 for reversible photocontrol of brain activity in mice via transcranial irradiation.

Conclusions

Due to the superior transmission through mammalian tissues, NIRW light can be harnessed to control biological processes in deep mammalian tissues. Because 700-nm photons penetrate through the human skull and brain tissues approximately 10- to 100-times better than 450-nm (blue) photons[2,28], external NIRW light can be applied noninvasively, without inserting fiber optics through the skull or creating cranial transparent windows[5,29,30]. The noninvasive transcranial optogenetic regulation of brain activities has previously been demonstrated in mice via the use of the red-shifted channelrhodopsins[31,32]. However, the absorption maxima of the most red-shifted rhodopsins is <600 nm, therefore their stimulation by the red light is inefficient[31]. Because absorption maxima of Bphs lie within the NIRW window, they are particularly attractive for noninvasive applications[33], including applications in the brain.

To our knowledge, this study represents the first demonstration of the use of a Bph-based system to control brain activity in live mammals. To accomplish this, we re-engineered the first generation NIRW-ACs, IlaC series[12], which proved to be inadequate for mammalian applications because of poor expression in mammalian cells and low activity at 37 °C. Poor expression was apparently due to the PSM from *R. sphaeroides* BphG1, whose replacement with the PSM from *D. radiodurans* BphP solved the expression problem. Low AC activity at 37 °C was due to the thermal instability of the AC module derived from CyaB1 from the mesophilic cyanobacterium, *Nostoc* sp. The replacement of this AC module with the AC module from Rv1264 derived from the pathogenic bacterium, *M. tuberculosis*, has resulted in hgher enzymatic activity at 37 °C. Ultimately, both PSM and AC modules of the first-generation NIRW-AC were replaced. The relative ease with which the PSM and AC modules can be combined to generate light-activated proteins lends support to the homodimeric Bph engineering principles described earlier[8,12]. The broad applicability of this approach is further demonstrated by engineered homodimeric Bphs containing AC modules from other bacteria as well as Bphs containing non-AC modules that function as homodimers[34–36].

At present, IlaM5 appears to be the most suitable NIRW-AC for mammalian applications. A recently engineered NIRW-AC of the PaaC series contains a cyanobacterial catalytic module and its AC activity is comparable to that of IlaC*[34]. A cyanobacteriophytochorme-based AC, cPAC, has lower photodynamic range, compared to IlaM5 and its performance at 37 °C has not been tested[37]. We demonstrated its applicability for light-dependent suppression of the spindle oscillations, a brain wave pattern characteristic of NREMS. Spindle waves are assumed to have two key functions: memory consolidation[38,39] and developmental refinement of brain circuits[40–42] during sleep. However, interrogating their exact functions has proved to be difficult because of the lack of tools to perturb them in sleeping mice. Because mice cannot see NIRW light[43], transcranial NIRW light irradiation represents an optimal means of manipulating sleep spindles in freely behaving animals. While IlaM5 expressed from an AAV vector resulted in robust and reversible light-dependent suppression

of the spindle oscillations, its expression and localization in the neurons may need to be optimized to minimize the observed undesired effects.

The omnipresence of cAMP signaling in mammals makes NIRW-ACs suitable for optogenetic applications in the tissues beyond the brain. Historically, finding pharmacological solutions to control cAMP signaling pathways in a tissue-specific manner has proved to be challenging. The scarcity of drugs that affect cAMP-dependent processes developed over the last few decades is a testament to the enormity of this challenge[15,16,18]. The temporary nature of cAMP signaling, which is difficult to capture by chemicals, represents yet another major challenge in using pharmacological approaches. The NIRW-AC optimized for mammalian applications represents a tool that may overcome many of these challenges and allow noninvasive regulation of cAMP signaling pathways in deep tissues, in cell-type specific manner and with temporal precision that is unmatched by drugs.

MATERIALS AND METHODS

Bacterial strains and growth conditions.

The bacterial strains and plasmids used in this study are listed in Supplementary Table 1. *E. coli* BL21[DE3] (NEB) and DH5α (NEB) and their derivatives were grown in LB medium supplemented with appropriate antibiotics at 28°C or 37 °C. When specified, irradiation was delivered by an LED All-red (660 nm) Grow Light panel (30.5 cm × 30.5 cm; LED Wholesalers) using repetitive cycles of 0.5 min light/ 2 min dark or 0.5 min light/ 30 min dark. Petri dishes were placed 10 cm above the light panel, at irradiance of ~0.2 mW cm^{-2}. For growth in the dark, Petri dishes were wrapped in aluminum foil.

Recombinant DNA techniques.

The genes encoding the NIRW-ACs were constructed using Gibson assembly according to the manufacturer's instructions (Gibson Assembly Master Mix, NEB). To construct genes of the IlaD series, the DNA fragment encoding aa 1–500 of the PSM of *bphP* (Gene ID: 1798221) was PCR-amplified from *D. radiodurans* genomic DNA and assembled with the fragment of plasmid pET23::ilaC22_k27_Y259, which carries a fragment of *cyaB1* (aa 585–857), the AC gene from *Nostoc* sp. To construct genes of the IlaM series, the *cyaB1* gene fragment in plasmid pET23::ilaD9 was replaced with the fragment encoding the AC catalytic domain (aa 211–397) from *M. tuberculosis Rv1264* (Gene ID: 887035), which was synthesized with codons optimized for *E. coli* (Eurofins Genomics). For neuronal expression, *ilaM5* (or *ilaC**) was cloned into the adeno-associated viral plasmid under the neuronal promoter *hSyn*, pAAV-hSyn-hChR2(H134R)-EYFP (gift from Karl Deisserhoth, Addgene #26973). The *hChR2(H134R)-EYFP* fragment was removed following digestion with *KpnI* and *AflI*, and the *ilaM5* (or *ilaC**), *bphO* (encoding the *R. sphaeroides* heme oxygenase[12]) and *eGFP* genes were inserted. Heme oxygenase was expressed to ensure sufficient BV levels in thalamic neurons. Sequences of *ilaM5* (or *ilaC**), *bphO* and *eGFP* were separated from each other by p2a sequences. All constructed plasmids were confirmed by DNA sequencing (Eurofins Genomics). The protein sequences of IlaD9 and IlaM5 are shown in Supplementary Fig. 6.

Screening system for bacterial AC activity.

AC activity screening was carried out based on the ability of heterologous ACs to complement the *cya* mutation of strain *E. coli* BL21[DE3] *cya* by increased expression of the chromosomal *lacZ* gene, as described earlier[12]. Overnight cultures containing two plasmids, pET23::AC and pT7-ho1[10], which encodes a cyanobacterial heme oxygenase HO1, were plated on LB agar containing 10–50 μM IPTG, 40 μM X-gal and the following antibiotics: 100 μg ampicillin (Ap) mL^{-1} and 25 μg kanamycin (Km) mL^{-1}. For the dark conditions, plates were covered in aluminum foil, while light-treated plates were placed 10 cm above All-Red (660 nm) LED Grow Light panel 225 (14W, 30.5 × 30.5 cm, LED Wholesalers, CA), where light irradiance at the plate surface was ~2 mW cm^{-2}. Irradiation regimens were either repetitive cycles of 0.5 min light/ 2 min dark or 0.5 min light/ 30 min dark. Plates were incubated at 28 °C for 40 h, and at 37 °C for 20 h.

Protein purification.

The NIRW-AC proteins (IlaC*, IlaD9, IlaM4 and IlaM5) carrying C-terminal His_6-tags were purified using TALON metal resin according to the manufacturer's protocol (Clontech) with few modifications. To avoid photobleaching or undesired AC photoactivation, protein expression and purification were performed under non-activating green light. Overnight cultures of *E. coli* BL21[DE3] containing two plasmids, pET23::AC and pT7-ho1, were grown in LB medium in the dark (wrapped in foil) supplemented with 100 μg Ap mL^{-1} and 25 μg Km mL^{-1}. The cultures were then diluted 1:50 into 200 mL of fresh LB medium and grown at 37 °C until A_{600} 0.5, at which point protein expression was induced by adding 0.5 mM IPTG (final concentration) and the cultures were grown under shaking at room temperature for an additional 12 h. Cells were collected by centrifugation at 4,000 × g for 10 min and resuspended in binding buffer (50 mM sodium phosphate, 300 mM NaCl, 10 mM imidazole, and protease inhibitor cocktail (Sigma). Cells were lysed using a French press, sonicated to disrupt DNA, and centrifuged at 8,000 × g for 15 min to remove insoluble cell debris. Soluble cell lysates were loaded onto 0.5 mL of TALON resin and incubated for 2 h at 4 °C. The resin was washed with 3 volumes of binding buffer and eluted with 0.3 mL elution buffer (50 mM sodium phosphate, 300 mM NaCl, 250 mM imidazole). The protein was either used immediately or stored at –20 °C following addition of 20% (v/v) glycerol (final concentration). Protein concentrations were measured using a Bradford protein assay kit (Bio-Rad) with bovine serum albumin as the protein standard. Protein purity was analyzed using SDS-PAGE.

Spectroscopy.

The absorption spectra of P_f and P_{fr} states of ACs were measured with a UV-1601 PC UV-visible spectrophotometer (Shimadzu) at room temperature. For activation of the P_r to P_{fr} conversion, protein solutions were irradiated with red light (All-Red (660 nm) LED Grow Light panel 225, at ~1 mW cm^{-2}) for 3 min. For the P_{fr} to P_r conversion, we used a custom made LED panel (3 W LED, 775 nm, Shenzhen Justar Electronic Technology).

AC enzymatic assays.

The AC assays were performed at room temperature (22 °C) and 37 °C as described[12]. Briefly, a reaction mixture (300 μL) contained 1 μM enzyme in an assay buffer optimized for the specific AC: a Mg^{2+}-based buffer (50 mM Tris-HCl [pH 8.0], 10% glycerol, 10 mM $MgCl_2$)[11] for the ACs containing CyaB1 (IlaC- and IlaD-series), or a Mn^{2+}-based buffer (50 mM Tris-HCl [pH 8.0], 20% glycerol, 3 mM $MnCl_2$)[22] for the ACs containing Rv1264 (IlaM-series). AC activity in the dark (P_r) state was measured under dim green light. AC activity of the lit (P_{fr}) state was measured in the solutions that were exposed to 1-min irradiation with red (660 nm, at ~1 mW cm^{-2}) light, and that were kept under light for the duration of the assay. The enzymatic reaction was started by the addition of 100 μM ATP (final concentration). Aliquots of 50 μL were withdrawn at 2.5, 10 and 30 min and boiled for 3 min for AC inactivation. The cAMP concentrations were measured using a cAMP ELISA kit (Enzo) according to the manufacturer's instructions. Chemiluminescent signal was measured with Synergy H4 microplate reader (BioTek Instruments).

NIRW-AC expression in HEK293 cells.

Human embryonic kidney (HEK293, ATCC RL-1573) cells were cultured in Eagle's Minimum Essential Medium (ATCC), supplemented with 10% (v/v) fetal bovine serum (FBS, Sigma) and 1% (v/v) penicillin/streptomycin solution (Sigma). The HEK293 cells were cultured at 37 °C in a humidified atmosphere containing 5% CO_2 and were regularly verified against *Mycoplasma* and bacterial contamination. For transfection, 5×10^4 cells were seeded in 24-well cell culture plates in colorless EMEM media lacking a pH indicator (VWR). After 20 h of incubation, cells were co-transfected with pAAV::IlaM5, pAAV::IlaC*, or empty AAV vector (pAAV::GFP), and a reporter plasmid, pCRE-MetLuc2, which expresses the secreted luciferase under the cAMP-dependent promoter (Clontech [TaKaRa], Catalog No. 631745), at 1:1 (w/w) ratio. Transfection was performed with JetPrime transfection reagent with 2:1 JetPrime:DNA mixture (w/w), containing 0.6 μg total plasmid DNA, according to the manufacturer's instructions (Polyplus). At 24 h post-transfection, the culture medium was replaced with fresh colorless EMEM medium (500 μL), and one plate was placed under All-Red (660 nm) LED Grow Light panel and irradiated with red light (1 min light/ 5 min dark) at irradiance of ~1 mW cm^{-2}, while another plate was incubated in the dark (covered in aluminum foil). Culture medium (20 μL) was withdrawn and collected at 3, 6, 12 and 24 h. Luciferase activity was assayed using *Gaussia* Luciferase Flash Assay Kit (Thermo Fisher) and measured on Synergy H4 microplate reader (BioTek Instruments). The luciferase values were normalized per eGFP fluorescence, which was measured at the final, 24 h, time point. In brief, cells were washed with PBS (Sigma), trypsinized with color-free 1x trypsin solution (Sigma), and the fluorescent signal from collected samples was measured on Synergy H4 microplate reader. Data represent the mean ± SD of three independent experiments.

AAV injection *in vivo*.

The pAAV-IIaM5 vector was custom packaged into AAV (serotype 1) and produced at the University of North Carolina at Chapel Hill Vector Core with a total titer of 1×10^{11} virus particles mL^{-1}. For virus injection, standard rodent anesthetic procedure and stereotaxic

device were used. Virus, 30–100 nL, was injected into the VPM region (stereotaxic coordinates: lateral and posterior both 1500 μm, ventral 3500–3000 μm) via a homemade microinjector, which is composed of a capillary glass micropipette, a wire plunger connected to a Narishige micromanipulator, in a 20 min period on a mouse stereotaxic device. Mice were anesthetized with oxygenated isoflurane during the entire process. Mice were allowed 2 weeks to recover and subsequently used for *in vivo* recording or brain slice electrophysiology studies. All experiments were performed under protocols approved by the IACUC committee of the University of Wyoming.

EEG recordings in mice.

Two-month-old mice (CD-1 450 strain) of either sex were anesthetized under isoflurane anesthesia (2 %) mixed with medical oxygen and were secured in a stereotaxic frame. Polyimide-insulated stainless steel wires (125 μm; California Fine Wire Co.), and connecting pins (Digikey) were implanted into the S1 and ipsilateral VPM. A screw-free, glue-based, electrode assembly system that allows for long-term recordings was used[44,45]. A reference electrode was placed into the ipsilateral olfactory bulb area. Mice were returned to their cages after EEG implantation. EEG recordings were conducted over a 24-h cycle with simultaneous video behavior monitoring, and automated infrared activity tracking at a frequency of twice per month to minimize disturbances. Animals were able to move freely in the recording chamber, which was supplied with water gel. EEG signals were amplified via a differential AC amplifier (Model 1700, A-M system), digitized using 460 Power 1401, and analyzed using the Spike-2 program (Cambridge Electronic Design). Offline analysis was conducted using custom programs developed using MATLAB (Mathworks). The following EEG features were compared between sham-treated (injected with an empty AAV vector) and IIaM5-expressing (injected with AAV::ilaM5) mice. For transcranial irradiation, light was delivered by an LED panel (New Anjeet 300W LED Panel Grow Light Hydroponic System) that contains 100 3-W (nominal power) LEDs emitting NIRW light. All blue LEDs in the panel were replaced with 730-nm 3-W LEDs (Shenzhen Justar Electronic Technology, P.R. China). The panel was placed approximately 30 cm above the mouse cage floor.

Power spectrum.

We first estimated the power in several frequency ranges (δ: 1–4 Hz, θ: 4–8 Hz, α: 8–12 Hz, σ: 12–16 Hz and β: 16–24 Hz) for each electrode. EEG power was normalized to its baseline levels during the NREMS stage.

Supplementary Material

Refer to Web version on PubMed Central for supplementary material.

ACKNOWLEDGEMENTS

A.F. and M.G. were supported by grants NIBIB 5R21EB018539, NIGMS 2P20GM103432 and NIGMS 1P20GM121310. C.Z. and Q.Q.S. were supported by NINDS 5R01NS094550. We are grateful to Danny Burns for performing virus injections, to Yang Liu for I_h measurements, to Taylor Doherty for constructing and installing LED panels, to Grant Bowman and Donald Jarvis for access to imaging equipment, and to Amy Fluet for manuscript editing.

ABBREVIATIONS

AAV	adeno-associated virus
AC	adenylate cyclase
Bph	bacteriophytochrome
BV	biliverdin IXα
Ap	amicillin
EEG	electroencephalographic
HCN	hyperpolarized cyclic nucleotide-dependent ion channels
I_h	current derived from HCNs
IlaC*	IlaC22 k27 Y259F
Km	kanamycin
NIRW	near-infrared optical window
NREMS	non-rapid eye movement sleep
P_{fr}	far-red light absorbing state
P_r	red light-absorbing state
PSM	photosensory module
VPM	ventral posteromedial

REFERENCES

1. Weissleder R A clearer vision for in vivo imaging. Nat. Biotechnol 2001, 19, 316–317. [PubMed: 11283581]
2. Wan S, Parrish JA, Anderson RR & Madden M Transmittance of nonionizing radiation in human tissues. Photochem. Photobiol 1981, 34, 679–681. [PubMed: 6458827]
3. Henderson TA & Morries LD Near-infrared photonic energy penetration: can infrared phototherapy effectively reach the human brain? Neuropsychiatr. Dis. Treat 2015, 11, 2191–2208. [PubMed: 26346298]
4. Mühlhäuser WWD, Fischer A, Weber W & Radziwill G Optogenetics - bringing light into the darkness of mammalian signal transduction. Biochim. Biophys. Acta 2017, 1864, 280–292.
5. Hennessy M & Hamblin MR Photobiomodulation and the brain: a new paradigm. J. Opt 2017, 19, 13003.
6. Rockwell NC, Su YS & Lagarias JC Phytochrome structure and signaling mechanisms. Annu. Rev. Plant Biol 2006, 57, 837–858. [PubMed: 16669784]
7. Chernov KG, Redchuk TA, Omelina ES & Verkhusha VV Near-infrared fluorescent proteins, biosensors, and optogenetic tools engineered from phytochromes. Chem. Rev 2017, 117, 6423–6446. [PubMed: 28401765]
8. Gomelsky M, Ryu MH Near-infrared light-activated proteins. 2014. US Patent 8,835,399.
9. Bassler J, Schultz JE, Lupas AN Adenylate cyclases: Receivers, transducers, and generators of signals. Cel. Signal 2018, 46, 135–144.

10. Tarutina M, Ryjenkov DA & Gomelsky M An unorthodox bacteriophytochrome from *Rhodobacter sphaeroides* involved in turnover of the second messenger c-di-GMP. J. Biol. Chem 2006, 281, 34751–34758. [PubMed: 16968704]
11. Kanacher T, Schultz A, Linder JU & Schultz JE A GAF-domain-regulated adenylyl cyclase from *Anabaena* is a self-activating cAMP switch. EMBO J. 2002, 21, 3672–3680. [PubMed: 12110580]
12. Ryu MH et al. Engineering adenylate cyclases regulated by near-infrared window light. Proc. Natl. Acad. Sci. U. S. A 2014, 111, 10167–10172. [PubMed: 24982160]
13. Hansen RT, University of Pennsylvania, personal communication. 2016.
14. Steegborn C Structure, mechanism, and regulation of soluble adenylyl cyclases - similarities and differences to transmembrane adenylyl cyclases. Biochim Biophys Acta. 2014, 1842, 2535–2547. [PubMed: 25193033]
15. Wahlang B, McClain C, Barve S & Gobejishvili L Role of cAMP and phosphodiesterase signaling in liver health and disease. Cell Signal. 2018, 49, 105–115. [PubMed: 29902522]
16. Heckman PRA, Blokland A, Bollen EPP & Prickaerts J Phosphodiesterase inhibition and modulation of corticostriatal and hippocampal circuits: Clinical overview and translational considerations. Neurosci. Biobehav. Rev 2018, 87, 233–254. [PubMed: 29454746]
17. Kim GE & Kass DA Handbook Exp. Pharmacol 2017, 243, 249–269.
18. Sakkas LI, Mavropoulos A & Bogdanos DP Phosphodiesterase 4 Inhibitors in immune-mediated diseases: mode of action, clinical applications, current and future perspectives. Curr. Med. Chem 2017, 24, 3054–3067. [PubMed: 28554321]
19. Bhoo SH, Davis SJ, Walker J, Karniol B & Vierstra RD Bacteriophytochromes are photochromic histidine kinases using a biliverdin chromophore. Nature 2001, 414, 776–779. [PubMed: 11742406]
20. Takala H, Björling A, Berntsson O et al. Signal amplification and transduction in phytochrome photosensors. Nature 2014, 509, 245–248. [PubMed: 24776794]
21. Burgie ES, Wang T, Bussell AN et al. Crystallographic and electron microscopic analyses of a bacterial phytochrome reveal local and global rearrangements during photoconversion. J. Biol. Chem 2014, 289, 24573–24587. [PubMed: 25006244]
22. Linder JU, Schultz A & Schultz JE Adenylyl cyclase Rv1264 from *Mycobacterium tuberculosis* has an autoinhibitory N-terminal domain. J. Biol. Chem 2002, 277, 15271–15276. [PubMed: 11839758]
23. Bruce AW, Donaldson IJ, Wood IC et al. Genome-wide analysis of repressor element 1 silencing transcription factor/neuron-restrictive silencing factor (REST/NRSF) target genes. Proc. Natl. Acad. Sci. U. S. A 2004, 101, 10458–63. [PubMed: 15240883]
24. Markova SV, Golz S, Frank LA, Kalthof B & Vysotski ES Cloning and expression of cDNA for a luciferase from the marine copepod *Metridia longa*: a novel secreted bioluminescent reporter enzyme. J. Biol. Chem 2004, 279, 3212–3217. [PubMed: 14583604]
25. Sartiani L, Mannaioni G, Masi A, Novella Romanelli M & Cerbai E The hyperpolarization-activated cyclic nucleotide-gated channels: from biophysics to pharmacology of a unique family of ion channels. Pharmacol. Rev 2017, 69, 354–395. [PubMed: 28878030]
26. Sun QQ, Prince DA & Huguenard JR Vasoactive intestinal polypeptide and pituitary adenylate cyclase-activating polypeptide activate hyperpolarization-activated cationic current and depolarize thalamocortical neurons in vitro. J. Neurosci 2003, 23, 2751–2758. [PubMed: 12684461]
27. Lüthi A Sleep spindles: where they come from, what they do. Neuroscientist 2014, 20, 243–56. [PubMed: 23981852]
28. Eggert HR & Blazek V Optical properties of human brain tissue, meninges, and brain tumors in the spectral range of 200 to 900 nm. Neurosurgery 1987, 21, 459–464. [PubMed: 3683777]
29. Boyden ES, Zhang F, Bamberg E, Nagel G & Deisseroth K Millisecond-timescale, genetically targeted optical control of neural activity. Nat. Neurosci 2005, 8, 1263–1268. [PubMed: 16116447]
30. Galvan A, Caiola MJ & Albaugh DL Advances in optogenetic and chemogenetic methods to study brain circuits in non-human primates. J. Neural Transm 2017, 1–17.
31. Lin JY, Knutsen PM, Muller A, Kleinfeld D & Tsien RY ReaChR: a red-shifted variant of channelrhodopsin enables deep transcranial optogenetic excitation. Nat. Neurosci 2013, 16, 1499–1508. [PubMed: 23995068]

32. Chuong AS, Miri ML, Busskamp V et al. Noninvasive optical inhibition with a red-shifted microbial rhodopsin. Nat. Neurosci 2014, 17, 1123–9. [PubMed: 24997763]
33. Chernov KG, Redchuk TA, Omelina ES & Verkhusha VV Near-infrared fluorescent proteins, biosensors, and optogenetic tools engineered from phytochromes. Chem. Rev 2017, 117, 6423–6446. [PubMed: 28401765]
34. Etzl S, Lindner R, Nelson MD & Winkler A Structure-guided design and functional characterization of an artificial red light–regulated guanylate/adenylate cyclase for optogenetic applications. J. Biol. Chem 2018, 293, 9078–9089. [PubMed: 29695503]
35. Ryu MH & Gomelsky M Near-infrared light responsive synthetic c-di-GMP module for optogenetic applications. ACS Synth. Biol 2014, 3, 802–810. [PubMed: 24926804]
36. Gasser C, Taiber S, Yeh CM et al. Engineering of a red-light-activated human cAMP/cGMP-specific phosphodiesterase. Proc. Natl. Acad. Sci. U. S. A 2014, 111, 8803–8808. [PubMed: 24889611]
37. Blain-Hartung M, Rockwell NC, Moreno MV et al. Cyanobacteriochrome-based photoswitchable adenylyl cyclases (cPACs) for broad spectrum light regulation of cAMP levels in cells. J. Biol. Chem 2018, 293, 8473–8483. [PubMed: 29632072]
38. Gais S, Mölle M, Helms K & Born J Learning-dependent increases in sleep spindle density. J. Neurosci 2002, 22, 6830–6834. [PubMed: 12151563]
39. Mednick SC, McDevitt EA, Walsh JK et al. The critical role of sleep spindles in hippocampal-dependent memory: a pharmacology study. J. Neurosci 2013, 33, 4494–4504. [PubMed: 23467365]
40. Cirelli C & Tononi G Cortical development, electroencephalogram rhythms, and the sleep/wake cycle. Biol. Psychiatry 2015, 77, 1071–1078. [PubMed: 25680672]
41. Tononi G & Cirelli C Sleep and the price of plasticity: from synaptic and cellular homeostasis to memory consolidation and integration. Neuron 2014, 81, 12–34. [PubMed: 24411729]
42. Muller L, Piantoni G, Koller D et al. Rotating waves during human sleep spindles organize global patterns of activity that repeat precisely through the night. eLife 2016, 5, pii: e17267 . [PubMed: 27855061]
43. Peirson SN, Brown LA, Pothecary CA, Benson LA & Fisk AS Light and the laboratory mouse. J. Neurosci. Methods 2018, 300, 26–36. [PubMed: 28414048]
44. Wu C, Wais M, Sheppy E, del Campo M & Zhang L A glue-based, screw-free method for implantation of intra-cranial electrodes in young mice. J. Neurosci. Methods 2008, 171, 126–131. [PubMed: 18420280]
45. Seelke AMH & Blumberg MS The microstructure of active and quiet sleep as cortical delta activity emerges in infant rats. Sleep 2008, 31, 691–699. [PubMed: 18517038]
46. Busby S & Ebright RH Transcription activation by catabolite activator protein (CAP). J. Mol. Biol 1999, 293, 199–213. [PubMed: 10550204]

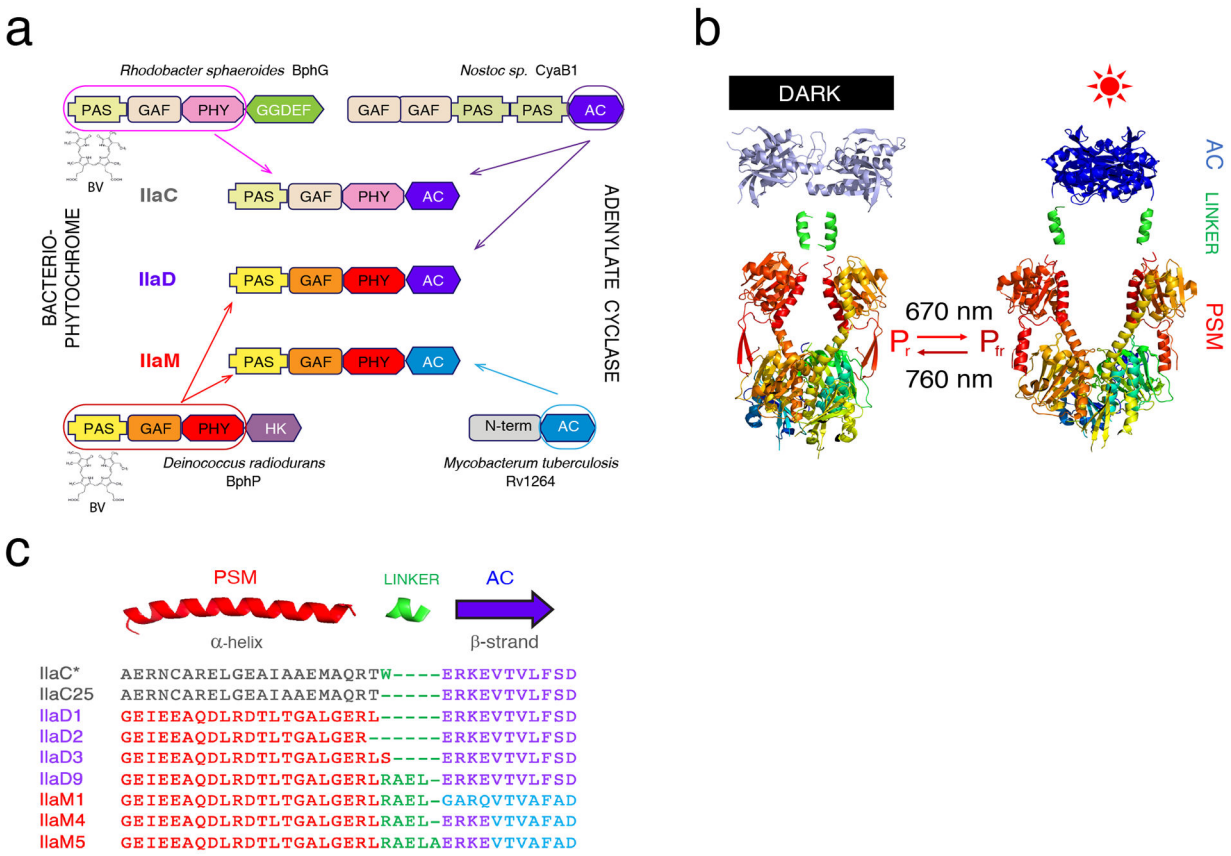

Figure 1. NIRW-ACs design.

(a) Domain architecture of the first (IlaC), second (IlaD), and third (IlaM) generations of NIRW-ACs. AC (type III AC catalytic domain), GAF, PAS, PHY, GGDEF (diguanylate cyclase catalytic domain), and HK (histidine kinase) are domain designations. The chromophore BV is covalently bound to the Cys residue in the PSM. **(b)** Chimeric Bph engineering. Shown are X-ray structures of the *D. radiodurans* BphP PSM (PAS-GAF-PHY) in its dark (left, PDB 4O0P) and light-activated (right, PDB 4O01) forms. Also shown are structures of *M. tuberculosis* AC RV1264 in the inactive (left, PDB 1Y10) and active (right, PDB 1Y11) conformations. The α-helices extending from the PSM are linked to the output AC modules to generate light-activated enzymes. **(c)** NIRW-AC protein sequences at the fusion of the PSM and AC modules. The amino acid colors correspond to the colors of protein domains shown above the protein sequences. PSM modules are shown in red (BphP) or grey (BphG1); AC domains are shown in violet (CyaB1) or blue (RV1264); added interdomain linkers are shown in green.

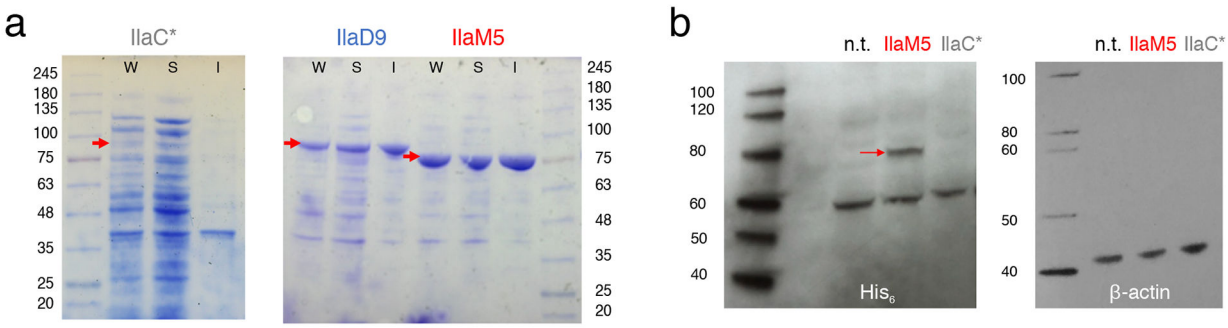

Figure 2. NIRW-AC expression in (a) *E. coli* and (b) human HEK293 cells.

(a) *E. coli* BL21 [DE3] *cya* cells carrying pET23::AC, where AC was either IlaC* (IlaC22 k27 Y259F), IlaD9 or IlaM5, and a plasmid expressing heme oxygenase, pT7-ho1[12]. Cells were collected post-induction with IPTG, as described in Material and Methods. Loaded are whole cell extracts (W), soluble (S) and Insoluble (I) fractions. Red arrows point to the position of the NIRW-AC protein bands. **(b)** HEK293 cells transfected with equal amounts of either pAAV::ilaC* or pAAV::ilaM5 DNA and grown for 24 h prior to collection. Equal amounts of total soluble protein from each culture were analyzed using SDS-PAGE. Left panels, NIRW-AC protein abundance assayed via Western blotting using a His_6-specific antibody. Right panel, β-actin-specific antibody used to verify equal protein loading. Molecular mass markers (kD) are shown on the sides of each panel. n.t., not transfected.

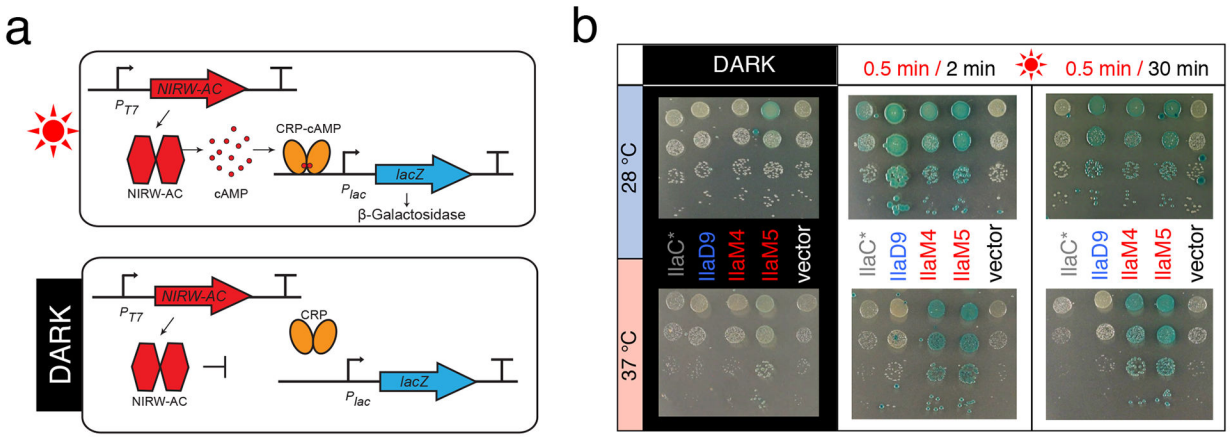

Figure 3. NIRW light and cAMP-dependent gene expression in *E. coli* expressing engineered ACs.

(a) The AC assay is based on the cAMP-CRP-dependent *lacZ* expression in the *E. coli cya* mutant[12]. CRP is a cAMP-dependent transcription activator[46]. **(b)** Images of AC-dependent β-galactosidase activity. *E. coli* BL21[DE3] *cya* carrying plasmids for expression of the NIRW-AC, pET23::AC, and heme oxygenase, pT7-ho1[10]. Strains were grown on LB agar containing X-Gal (40 μM) and IPTG (25 μM), either in the dark or in the red (660 nm) light.

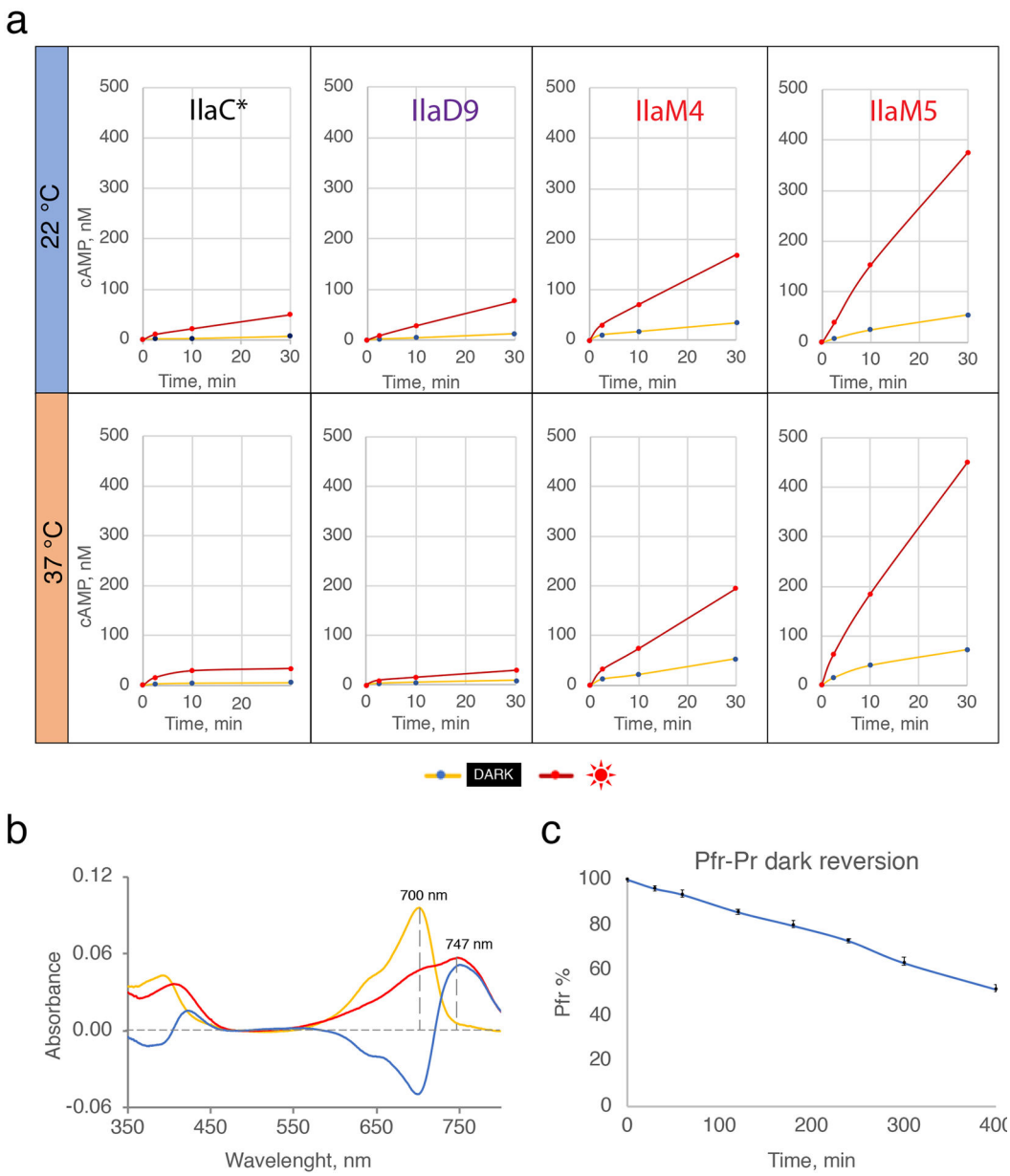

Figure 4. Photochemical characterization of NIRW-AC variants *in vitro*.

(a) Kinetics of cAMP accumulation by the purified IlaC*, IlaD9, IlaM4 and IlaM5 proteins in the dark and light, at 22 °C and 37 °C. Results of one experiment representative of three independent protein purifications are shown. **(b)** The UV-vis absorption spectra of IlaM5. **(c)** Kinetics of the dark recovery of IlaM5 from the lit P_{fr} state. Plotted are temporally changes in absorbance at 750 nm. Shown are averages from three technical replicates performed using one protein preparation.

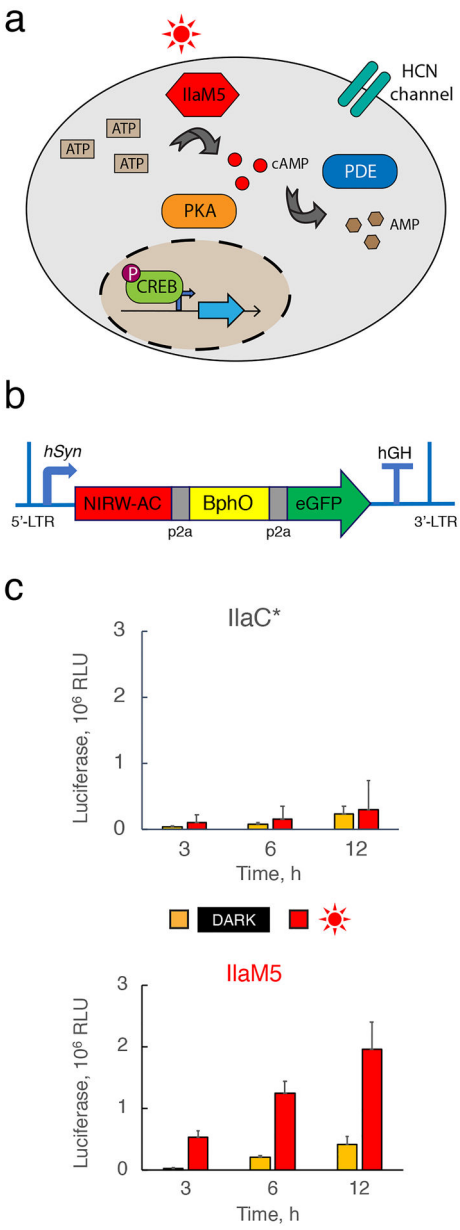

Figure 5. Light-activated cAMP synthesis by NIRW-ACs expressed in HEK293 cells.

(a) cAMP pathway in mammalian cells. **(b)** Adeno-associated viral construct encoding the NIRW-AC (either IlaC* or IlaM5), heme oxygenase BphO, and green fluorescent protein eGFP, used as transfection control from the neuronal *hSyn* promoter. **(c)** Comparison of NIRW-AC activities of IlaC* and IlaM5 expressed in HEK293 cells. Cell cultures expressing IlaC* or IlaM5 were irradiated with red (660 nm) light and changes in the cAMP levels were monitored by measuring secreted luciferase MetLuc expressed from the cAMP-dependent promoter. Shown are average data from three biological replicates, each performed in duplicate, ± standard deviation.

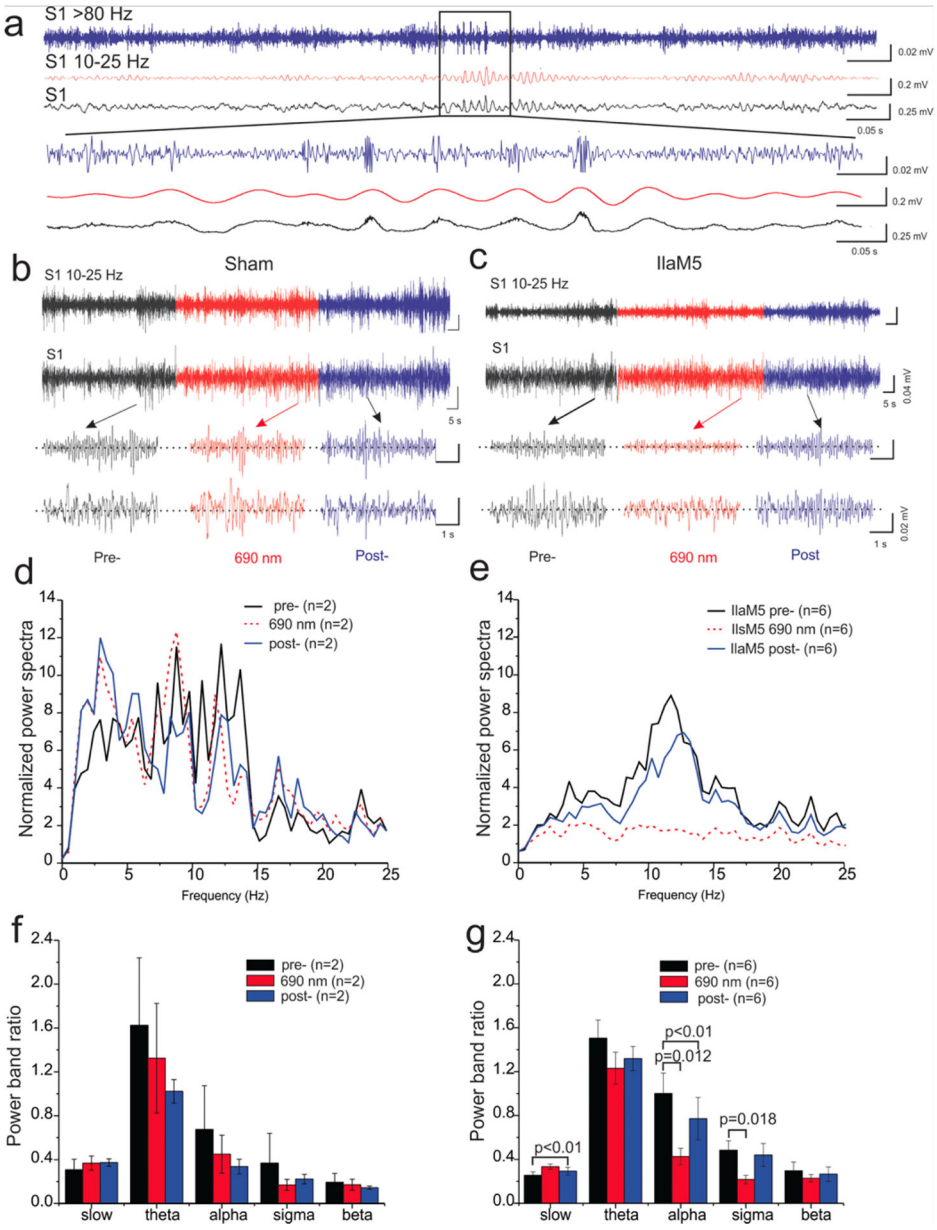

Figure 6. NIRW light-induced suppression of spindle waves in sleeping mice.

(a) EEG recordings of NREMS in S1. **(b-e)** Representative expanded EEG traces (b, c) and power- spectral of the EEG trace (d, e) pre-, during, and post NIRW irradiation in S1. **(f, g)** Effects of transcranial NIRW light stimulation via an LED panel on the power-band for spindle waves (10– 15 Hz) recorded in the S1. (b, d, f), sham (empty AAV injected); (c, e, g), IlaM5 expressing mice (AAV::ilaM5 injected).